Earth Syst. Sci. Data, 16, 5563–5578, 2024
https://doi.org/10.5194/essd-16-5563-2024

Open Access Earth System Science Data

Gas exchange velocities (k_{600}), gas exchange rates (K_{600}), and hydraulic geometries for streams and rivers derived from the NEON Reaeration field and lab collection data product (DP1.20190.001)

Kelly S. Aho[1,2], Kaelin M. Cawley[3], Robert T. Hensley[3], Robert O. Hall Jr.[4], Walter K. Dodds[5], and Keli J. Goodman[3]

[1]Department of Earth and Environmental Science, Michigan State University, East Lansing, MI 48824, USA
[2]Department of Integrative Biology, Michigan State University, East Lansing, MI 48824, USA
[3]National Ecological Observatory Network, Battelle, 1685 38th St. no. 100, Boulder, CO 80301, USA
[4]Flathead Lake Biological Station, University of Montana, Polson, MT 599111, USA
[5]Division of Biology, Kansas State University, Manhattan, KS 66506, USA

Correspondence: Kelly S. Aho (kellyaho@msu.edu)

Received: 30 July 2024 – Discussion started: 13 August 2024
Revised: 4 October 2024 – Accepted: 21 October 2024 – Published: 5 December 2024

Abstract. Air–water gas exchange is essential to understanding and quantifying many biogeochemical processes in streams and rivers, including greenhouse gas emissions and metabolism. Gas exchange depends on two factors, which are often quantified separately: (1) the air–water concentration gradient of the gas and (2) the gas exchange velocity. There are fewer measurements of gas exchange velocity compared to concentrations in streams and rivers, which limits accurate characterization of air–water gas exchange (i.e., flux rates). The National Ecological Observatory Network (NEON) conducts SF_6 gas-loss experiments in 22 of their 24 wadeable streams using standardized methods across all experiments and sites, and publishes raw concentration data from these experiments on the NEON data portal. NEON also conducts NaCl injections that can be used to characterize hydraulic geometry at all 24 wadeable streams. These NaCl injections are conducted both as part of the gas-loss experiments and separately. Here, we use these data to estimate gas exchange and water velocity using the reaRate R package. The dataset presented includes estimates of hydraulic parameters, cleaned raw concentration SF_6 tracer-gas data (including removing outliers and failed experiments), estimated SF_6 gas-loss rates, normalized gas exchange velocities (k_{600}; $\mathrm{m\,d^{-1}}$) and normalized depth-dependent gas exchange rates (K_{600}; $\mathrm{d^{-1}}$). This dataset provides one of the largest compilations of gas-loss experiments ($n = 339$) in streams to date. This dataset is unique in that it contains gas exchange estimates from repeated experiments in geographically diverse streams across a range of discharges. In addition, this dataset contains information on the hydraulic geometry of all 24 NEON wadeable streams, which will support future research using NEON aquatic data. This dataset is a valuable resource that can be used to explore both within- and across-reach variability in the hydraulic geometry and gas exchange velocity in streams. The data are available at https://doi.org/10.6073/pasta/18dcc1871ee71cf0b69f2ee4082839d0 (Aho et al., 2024), and the reaRate R package code is available at https://doi.org/10.5281/zenodo.12786089 (Cawley et al., 2024).

Published by Copernicus Publications.

1 Introduction

Air–water gas exchange contributes to many aquatic processes in streams and rivers, including greenhouse gas emissions (Liu et al., 2022; Rocher-Ros et al., 2023), aquatic metabolism (Aristegi et al., 2009; Hall et al., 2016; Hall and Hotchkiss, 2017), and reoxygenation rates after wastewater discharge (O'Connor and Dobbins, 1958). Despite this importance, gas exchange can be difficult to measure and model (Churchill et al., 1964; Hornberger and Kelly, 1975; Rathbun, 1977; Ulseth et al., 2019). According to Fick's law of diffusion, gas flux across the air–water boundary depends on the concentration gradient of the gas and the gas exchange velocity (k; $\mathrm{m\,d^{-1}}$):

$$\text{flux} = k\left(\left[\text{gas}\right]_{\text{dissolved}} - \left[\text{gas}\right]_{\text{equilibrium}}\right), \quad (1)$$

where $\left[\text{gas}\right]_{\text{dissolved}}$ is the concentration of the gas of interest, and $\left[\text{gas}\right]_{\text{equilibrium}}$ is the concentration of the gas at equilibrium with the atmosphere.

In streams and rivers, measurements of gas concentrations are more readily available than estimates of k; resultantly, estimates of k are often extrapolated from a few measurements. Several methods exist for assessing k, including predictive models (Raymond et al., 2012), models of gas dynamics through time and space in rivers (Appling et al., 2018), and direct measurements with tracers (Hall and Hotchkiss, 2017). Here, k refers to exchange of dissolved gases (i.e., diffusive and bubble-mediated gas transfer) and does not capture ebullitive fluxes. Characterizing k from direct measurement of tracer-gas exchange velocities and modeling based on observed diurnal gas dynamics are likely more accurate for any particular stream or river than more general predictive models (Appling et al., 2018; Hall and Ulseth, 2020; Riley and Dodds, 2013).

Gas exchange velocity is spatiotemporally variable; it is controlled by energy dissipation rate and, therefore, turbulence at the air–water boundary (Zappa et al., 2007). Models that estimate k at broad spatial scales and in low-versus-high gradient streams have found that hydraulic variables (e.g., streambed slope (S; unitless), water velocity (v; $\mathrm{m\,s^{-1}}$), mean water depth ($\bar{z}$; m), discharge (Q; $\mathrm{L\,s^{-1}}$)) are the dominant controls on variation in k (Churchill et al., 1964; O'Connor and Dobbins, 1958; Rathbun, 1977; Raymond et al., 2012). Although similar models for within-reach temporal variability are not widely available, hydrology is expected to control k locally. Existing reach-scale studies have reported different k responses to Q (Genzoli and Hall, 2016; Maurice et al., 2017; McDowell and Johnson, 2018) and point to the importance of quantifying the variable relationships between k and Q on a site-by-site basis. The dataset presented here leverages a unique set of tracer-gas experiments conducted by the National Ecological Observatory Network (NEON) that will allow for assessment of within- and across-reach variability in lotic gas exchange in a wide variety of streams.

Tracer-gas experiments are an approach to estimating k in streams and rivers and involve diffusing an inert tracer gas (e.g., sulfur hexafluoride (SF_6)) at a constant rate at the upstream end of a stream reach and measuring how concentrations decline downstream of the injection point. Often a conservative salt (e.g., sodium chloride (NaCl) or sodium bromide (NaBr)) is also injected with the tracer gas to allow for correction of dilution from hydrologic inflows (referred to as "salt correction" hereafter).

Here, we present a continental-scale dataset of gas exchange rates for wadeable streams derived from NEON data. The substantial processing that was required to estimate gas exchange is described in detail below and archived alongside the dataset. The dataset presented here contains estimates of k_{600}, or k normalized to a Schmidt number of 600, and K_{600}, which is a depth-corrected rate ($K_{600} = k_{600}/\bar{z}$) used in stream metabolism modeling, for 22 streams and v, $\bar{z}$, and at-a-station hydraulic geometry for 24 streams (Fig. 1).

2 Methods

2.1 NEON tracer-gas experiments

NEON conducts tracer-gas experiments at 22 stream sites, which are distributed across the United States, from Puerto Rico to Alaska (Fig. 1). For information about specific site characteristics, see the NEON website: https://www.neonscience.org/field-sites/explore-field-sites (last access: 2 October 2024). In general, the NEON streams are relatively small; the median watershed size is $11.5\,\mathrm{km^2}$, while the mean $\pm$ standard deviation watershed size is $27.5 \pm 58.5\,\mathrm{km^2}$. Walker Branch (WALK) drains the smallest watershed ($1.1\,\mathrm{km^2}$) while Sycamore Creek (SYCA), an intermittent, desert stream, drains the largest ($280\,\mathrm{km^2}$). Therefore, this dataset is only representative of streams and small rivers and not large rivers. These experiments entail continuous injections of SF_6 and a conservative salt tracer (either NaCl or NaBr) at the upstream end of a ≤ 500 m stream reach (Fig. 2). NEON uses SF_6 because it does not occur naturally, is not biologically or chemically reactive, and can be detected at low concentrations (Cole and Caraco, 1998; Ho et al., 2011; Maurice et al., 2017; Wanninkhof et al., 1985); although used in very small amounts in these experiments, SF_6 is a potent greenhouse gas, and tracer-gas experiments are ceasing at sites with sufficient hydrologic coverage. When NaBr is used as the salt tracer, an additional NaCl "slug" injection is performed, which allows for the subsequent calculation of v and the derivation of $\bar{z}$ from paired Q measurements (via flowmeter or acoustic Doppler current profiler, ADCP) and wetted width measurements taken at 30 points along the study reach. Before the injection, NaCl or NaBr is collected at each of the four stations along the study reach; these data can later be used to correct NaCl or NaBr concen-

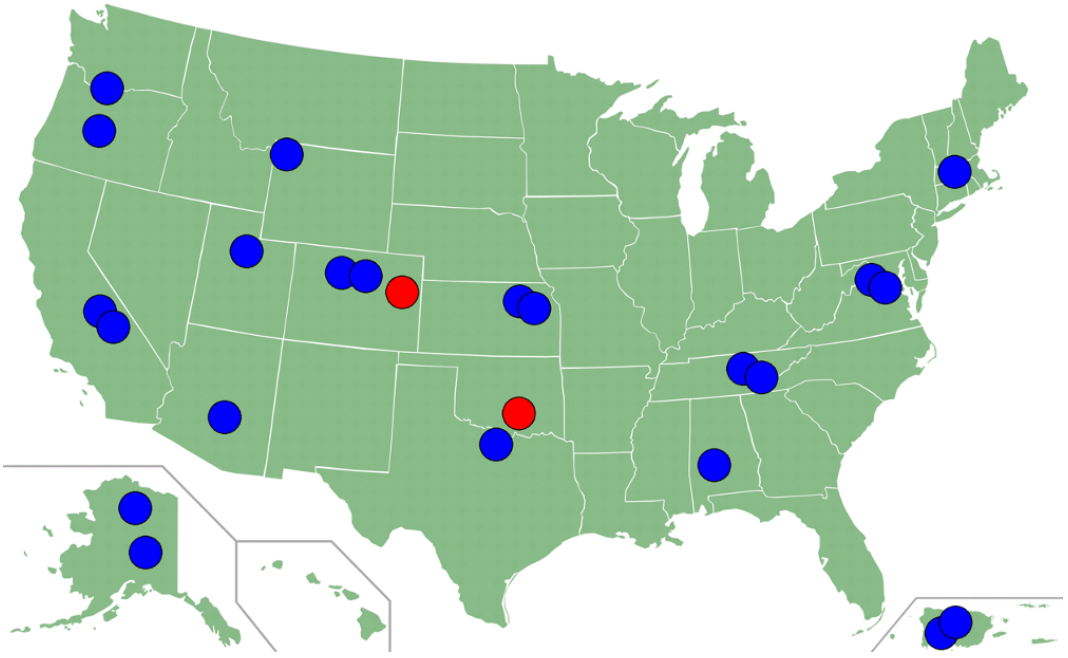

Figure 1. Map of NEON stream sites. Blue symbols indicate sites where NEON conducts full tracer-gas experiments and, thus, where we were able to estimate k_{600}, K_{600}, v, $\overline{z}$, and at-a-station hydraulic geometry. Red symbols indicate sites where NEON only conducts NaCl slug injections and, thus, where we were able to calculate v, $\overline{z}$, and at-a-station hydraulic geometry.

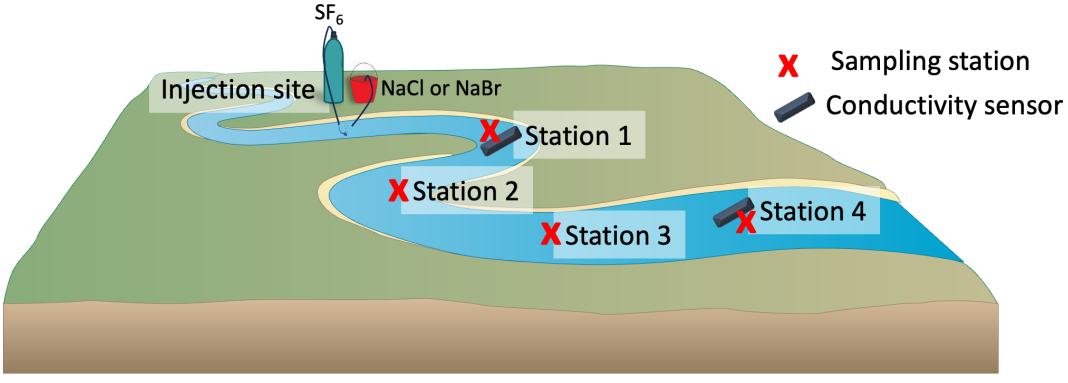

Figure 2. Diagram of a model study reach for NEON tracer-gas experiments. Each ∼ 500 m study reach comprises an injection site and four downstream sampling stations (Stations 1–4). At the upstream injection site, SF_6 is diffused into the water column with an air stone, and NaCl or NaBr is dripped into the stream. After plateau concentrations are reached at the downstream end of the study reach, injection rates are maintained, and field quintuplicate samples for SF_6 and NaCl or NaBr concentrations are collected at four downstream stations spaced along the study reach. At the upper and lower stations, conductivity sensors are deployed and used to monitor either (1) when NaCl plateau concentrations are reached (for NaCl continuous injections) or (2) when a NaCl "slug" peaks at each station (for NaBr continuous injections). Before each experiment, stream discharge is measured with a flow meter or ADCP, and 30 wetted widths are collected across the study reach. Also, before each injection, background NaCl or NaBr concentrations are collected at all four sampling stations. This diagram uses modified imagery from the University of Maryland Center for Environmental Science Integration and Application Network.

trations during the injection for background conditions. Once conductivity during the injection either reaches a plateau (for constant-rate NaCl injections) or returns to background levels (for NaCl slug injections) at the most downstream station, five replicate SF_6 and NaCl or NaBr samples are collected at each of the four stations located along the study reach. Samples for SF_6 are collected via headspace equilibration in 60 mL syringes, stored in gas-tight evacuated vials (12 mL, Exetainer), and run on a gas chromatograph with an electron capture detector (ECD). Samples for NaCl and NaBr are filtered to 0.7 µm, collected in 60 mL HDPE bottles, and run on an ion chromatograph. In addition, high-frequency (0.1 Hz) sensors are deployed to monitor NaCl conductivity at the upstream and downstream end of the study reach (Fig. 2).

NEON publishes SF_6 mixing ratios, NaCl and NaBr concentrations, wetted width data, and conductivity time series from these experiments as the Reaeration field and lab collection data product, DP1.20190.001 (NEON, 2024b), and measurements of Q in the Discharge field collection data product, DP1.20048.001 (NEON, 2024a). More detailed information on NEON's data collection procedures can be found on their website, http://www.neonscience.org (last access: 2 October 2024).

NEON has conducted tracer-gas experiments 6–10 times per year for 6–8 years at all 22 sites to capture a range of discharge conditions. Presently, tracer-gas experiments are ceasing at sites with sufficient hydrograph coverage (https://www.neonscience.org/impact/observatory-blog/protocol-change-reaeration-field-and-lab-collection-dp120190001, last access: 2 October 2024). However, NaCl slug injections will continue to be performed quarterly to collect high-frequency conductivity time-series data that allow for the calculation of v and the derivation of $\overline{z}$ from paired Q and wetted-width measurements. Similarly, NaCl slug injections are and will continue to be conducted for the two sites where tracer-gas experiments are not collected (Blue River (BLUE), where wide channel widths and high discharges make tracer-gas studies challenging, and Arikaree River (ARIK), where long travel times make tracer-gas studies infeasible).

The dataset presented here represents substantial processing of these published data (i.e., SF_6 mixing ratios, NaCl and NaBr concentrations, conductivity time series, wetted widths, and measurements of Q) to estimate k_{600} or K_{600} using the reaRate R package (Cawley et al., 2024). In addition, this dataset contains estimates of v from NaCl injections, which, as mentioned above, are performed both during tracer-gas experiments and at quarterly intervals at sites where tracer-gas experiments are not conducted or have ceased. Along with the paired Q measurement and the average wetted width for the study reach ($\overline{w}$; m), the estimate of v was used to derive $\overline{z}$. The dataset presented here contains estimates of v and $\overline{z}$ and at-a-station hydraulic geometry for all 24 NEON wadeable streams. This dataset provides a large compilation of direct measurements of tracer-gas experiments and at-a-station hydraulic geometry in small streams across the United States.

2.2 reaRate R package

The data processing pipeline described below uses the reaRate R package (Cawley et al., 2024). The package estimates k_{600} and K_{600} from data available on the NEON data portal. The package works by fitting an exponential, first-order decay function to the observed longitudinal decline in published SF_6 concentrations and solving for the longitudinal tracer-gas-loss rate (K_d; m^{-1}):

$$C_x = C_0 e^{-K_d x}, \tag{2}$$

where C_0 and C_x are tracer-gas concentrations at the top of the study reach and at a downstream point x, respectively, and K_d is the average distance traveled by an SF_6 molecule before it is emitted to the atmosphere. For sites where lateral inflows (e.g., groundwater inputs, overland flow, tributaries) appear to dilute SF_6 concentrations, the ratio of SF_6 to NaCl or NaBr is used to calculate a salt-corrected K_d value. The K_d values can then be converted to the gas exchange velocity for the tracer gas (e.g., k_{SF_6}; $m\,d^{-1}$):

$$k_{SF_6} = \overline{z} v K_d . \tag{3}$$

This gas-specific k can be normalized to k_{600} using a Schmidt number of 600:

$$k_{600} = k_{SF_6}\left(\frac{600}{Sc_{SF_6}}\right)^{-n}, \tag{4}$$

where n is the Schmidt number exponent (0.5 for flowing waters), and Sc_{SF_6} is the temperature-dependent Schmidt number for SF_6 at water temperature T in degrees Celsius (Jähne et al., 1987; Raymond et al., 2012; Wanninkhof, 1992):

$$Sc_{SF_6} = 3255.3 - 217.13T + 6.8370T^2 - 0.086070T^3. \tag{5}$$

Reporting estimates of k_{600} is common; it allows for comparisons with existing work and can be scaled to other gases, including CO_2 and O_2, using the same approach as in Eq. (4) with gas-specific, temperature-dependent Schmidt numbers:

$$k_{gas} = k_{600}\left(\frac{Sc_{gas}}{600}\right)^{-\frac{1}{2}}. \tag{6}$$

Some applications (e.g., metabolism, reoxygenation rates) explicitly include water depth in their modeling frameworks and thus require a depth-dependent gas exchange rate (K; d^{-1}). In these cases, a normalized gas exchange rate (K_{600}) can be used and is related to k_{600} by dividing by $\overline{z}$ for the upstream reach corresponding to a length of at least $\frac{1}{K_d}$. Using the same scaling relationships shown in Eqs. (3) and (5), K_{600} can be converted to gas-specific K_{gas} estimates.

The reaRate package uses NaCl breakthrough curves (i.e., from either continuous injection or slug injections) to estimate the travel time between the upstream and downstream stations and then calculates v as the distance between stations divided by the travel time. Using the continuity equation, $\overline{z}$ is calculated by dividing Q by v and $\overline{w}$. Finally, k_{SF_6} and K_{SF_6} are calculated from K_d, v, and $\overline{z}$ (Eq. 3) and then normalized to k_{600} and K_{600} (Eq. 4). The reaRate package includes two approaches to estimate k_{600} and K_{600}: an un-pooled frequentist approach and a partially pooled Bayesian approach, both of which are described in more detail below. Implementation of the package and all processing described below were conducted in R 4.2.3 (R Core Team, 2023). More information about the package, including details about the individual functions and a processing pipeline, is provided in Sect. 2.3.

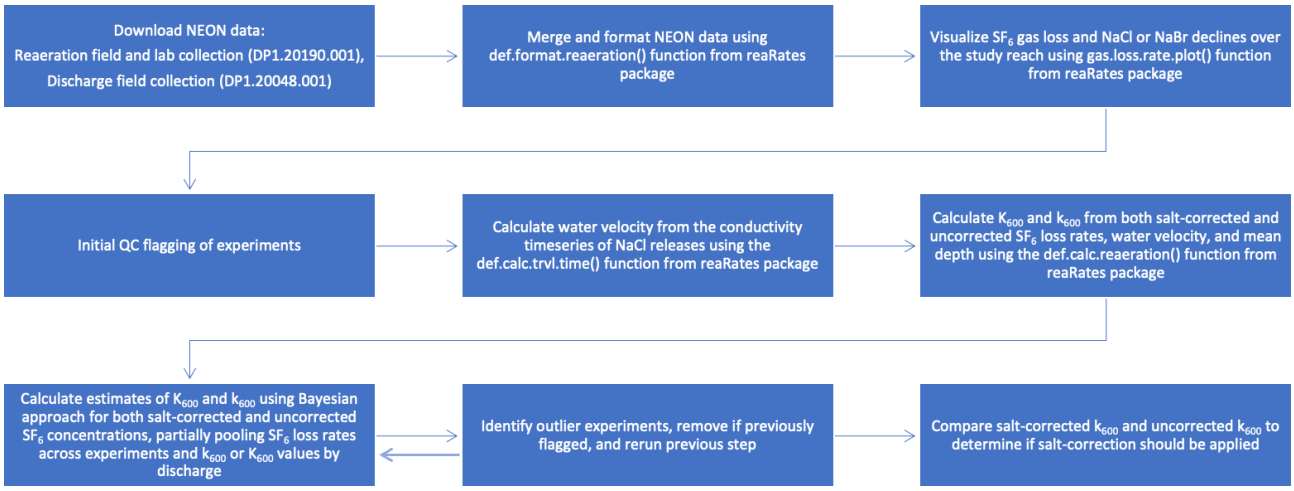

Figure 3. Overview of data processing to estimate k_{600} and K_{600} from NEON tracer-gas experiments.

2.3 Data processing

Substantial processing was required to estimate k_{600} and K_{600} from the NEON data (Fig. 3). All data used were downloaded from the NEON data portal. Downloads consisted of two NEON data products: Reaeration field and lab collection (DP1.20190.001) and Discharge field collection (DP1.20048.001). Data were from RELEASE-2023, in addition to nine experiments that were provisional but are now included in RELEASE-2024 (NEON, 2023a, b, 2024a, b). On a site-by-site basis, data were merged and formatted using the `def.format.reaeration()` function from the reaRate R package. This function compiles variables from across the downloaded data into a single data frame. These variables include Q, $\overline{w}$, water temperature, station location as a distance downstream from the injection point, and SF_6 and NaCl or NaBr concentrations for each station during the experiment. The function also applies a salt correction to the SF_6 data (e.g., SF_6 concentration divided by background-corrected NaCl or NaBr concentrations). The function removes outliers (points more extreme than $1.5 \times$ IQR below and above the first and third quartile, respectively) from the quintuplet SF_6 and NaCl or NaBr concentrations for each station, calculates the mean and standard deviation SF_6 and NaCl or NaBr concentration for each station, and flags stations as "unmixed" when the coefficient of variation ($CV = \frac{SD}{mean}$) of the replicate SF_6 and NaCl or NaBr concentrations is greater than 10 %.

Next, SF_6 and NaCl or NaBr declines were visualized and quantified for each experiment and initial quality control flags were assigned. The `gas.loss.rate.plot()` function from the reaRate package was used to visualize and calculate both salt-corrected and uncorrected longitudinal gas-loss rates over the length of the study reach (K_d). For the sites requiring a salt correction to account for lateral inflows, mean SF_6 mixing ratios at each station were first divided by mean background-corrected NaCl or NaBr concentration for the corresponding station. Station-specific outliers (i.e., values more extreme than first quartile $-1.5 \times$ IQR and third quartile $+1.5 \times$ IQR) were removed. SF_6 concentrations were then log-normalized, and K_d was calculated from the result-

Table 1. Sites and number of experiments.

Site name	NEON site ID	Velocity experiments (n)	Tracer-gas experiments (n)
Arikaree River	ARIK	22	0
Upper Big Creek	BIGC	28	24
Blacktail Deer Creek	BLDE	17	15
Blue River	BLUE	21	0
Caribou Creek	CARI	38	34
Como Creek	COMO	37	33
Rio Cupeyes	CUPE	41	41
Rio Guilarte	GUIL	42	40
Lower Hop Brook	HOPB	45	40
Kings Creek	KING	19	14
LeConte Creek	LECO	37	31
Lewis Run	LEWI	46	40
Martha Creek	MART	33	31
Mayfield Creek	MAYF	43	43
McDiffett Creek	MCDI	32	18
McRae Creek	MCRA	28	26
Oksrukuyik Creek	OKSR	38	34
Posey Creek	POSE	44	39
Pringle Creek	PRIN	14	13
Red Butte Creek	REDB	39	39
Sycamore Creek	SYCA	20	19
Teakettle 2 Creek	TECR	21	18
Walker Branch	WALK	47	43
West St Louis Creek	WLOU	39	34

ing linear decline. A quality control flag was assigned to an individual experiment if any of the following criteria applied:

- Visually, the SF_6 gas-loss rate over the entire study reach was unduly affected by anomalous SF_6 concentrations (potentially indicating contamination, leaked vials, or analytical error).
- SF_6, NaCl, or NaBr concentrations increased in a downstream direction between any of the stations (likely indicating incomplete mixing in the water column).
- The salt-corrected K_d was larger than the uncorrected K_d (a salt correction should correct for overestimation due to lateral inflows, with the reverse potentially indicating contamination or analytical error).

For each experiment, v was calculated from the conductivity time series using the `def.calc.trvl.time()` function. The function requires that the user manually selects points bracketing either the rising limb (for constant rate injections) or the peak concentration (for slug injections). From within the user-selected bracket, the `def.calc.trvl.time()` function smooths the data using a loess function and then identifies the peak of the breakthrough by finding either where the first derivative is 0 (for a slug injection) or where it is at its maximum (for a constant rate injection). This function then calculates the breakthrough travel time between the two stations and uses the distance between stations to calculate v. Site-specific relationships between v and Q were visualized in log–log space, and any anomalous values were reprocessed with the `def.calc.trvl.time()` to confirm that the user-selected bracketing allowed the function to pick the correct points on the time series. Finally, $\overline{z}$ was calculated using the `def.calc.trvl.time()` function, which divides Q by v and $\overline{w}$.

Two separate approaches were used to estimate k_{600} or K_{600} values from the formatted data. The first approach used the `def.calc.reaeration()` function to multiply K_d for each individual experiment by the corresponding v and $\overline{z}$ values (Eq. 3) to estimate k_{SF_6}, which were then converted to k_{600} (Eq. 4). The resulting k_{600} estimates were converted to K_{600} by dividing by water depth. This approach is subsequently referred to as the un-pooled, frequentist approach and is included in this data descriptor because it represents the current, prevailing approach for processing this type of data, is straightforward to implement, and represents the output of the `def.calc.reaeration()` function included in the reaRate package.

The second approach used Bayesian multilevel models that pooled experiments from the same site across releases. The models, coded in the Stan probabilistic programming language, used for this approach are also included in the reaRate package. A Bayesian approach provides flexibility in specifying models that consider repeat experiments at a site and current theory surrounding gas exchange. Bayesian inference allowed partial pooling of k_{600} estimates across releases in any one stream. Partial pooling reduces the error in any one estimate of k_{600} and shrinks all k_{600} estimates to the site-level mean (as conditioned on discharge) if error in measuring SF_6, NaCl, and/or NaBr is high.

The Bayesian approach included error at two levels. First, the models pooled k_{600} estimates across releases from the same site to estimate K_d from normalized SF_6 concentrations (both salt-corrected and uncorrected). For this step, the relationship between the SF_6 loss rate and the product of K_d and reach length was assigned a prior normal distribution with a normally distributed sigma (0, 0.2) and intercept (0, 0.1). We fully pooled the intercept with a strong prior near 0 because all SF_6 concentrations (i.e., measurements from Stations 1–4) were normalized to the SF_6 concentration at Station 1; this approach means that the intercept should be near 1, or 0 when logged. Thus, the model fit can be described as variable-slope, fixed-intercept linear regression. Second, the models pooled the estimates of k_{600} and K_{600} by Q, using linear relationships between Q and k_{600} or K_{600}. Priors were assigned for both the slope and the intercept based on predictions from an existing scaling model (Eq. 4 in Raymond et al., 2012). These priors were given large variances when possible (i.e., 10 for the intercept and 1 for the slope) to allow for divergence from the model predictions. However, at sites with a limited number of experiments (e.g., Pringle Creek, PRIN, and Kings Creek, KING), we used smaller variances to allow the model to converge. The site-specific priors used are listed in Table S1.

The two levels described can be referred to as a within-release model and an among-release model. The within-release model was a log-transformed (base e) exponential model. We log-transformed the model because SF_6 is always positive (ambient = 0) and because errors in the measurement of SF_6 can scale with the magnitude of the concentration.

$$\log\left(S_{i,j}\right) = \log\left(S_0\right) - K_{D,j}x_{i,j} + \varepsilon_{i,j}$$

and

$$\varepsilon_{i,j} \sim \text{normal}\left(0, \sigma_{\text{release}}\right),$$

where $S_{i,j}$ is the SF_6 concentration normalized to the concentration at Station 1 for any one release (sample i in release j), S_0 is the normalized SF_6 concentration at Station 1, $x_{i,j}$ is the distance downstream to which the normalized concentration corresponds, and $\varepsilon_{i,j}$ is a normally distributed random variable with $\mu = 0$ and $\text{SD} = \sigma_{\text{release}}$. We then converted $K_{D,j}$ to gas exchange velocity $k_{SF_6,j}$ using Eq. (3) and normalized to $k_{600,j}$ using Eq. (4). The among-release model included a linear model predicting the parameter $k_{600,j}$ as a linear function of discharge:

$$\log\left(k_{600,j}\right) = a + b \times \log\left(Q_j\right) + \varepsilon_j$$

and

$$\varepsilon_j \sim \text{normal}\left(0, \sigma_{\text{stream}}\right),$$

where a and b are the intercept and slope parameters of a model regressing $\log\left(k_{600,j}\right)$ and $\log\left(Q_j\right)$, where Q_j is the discharge during any one release and σ_{stream} is the residual variation. We also fit linear second-level models with $\log\left(K_{600,j}\right)$, where $K_{600,j}$ is the per-time gas exchange rate.

We fit models using Stan in the RStan package in R (Stan Development Team, 2023). The models were run for at least 5000 iterations over four chains. Models were assessed according to the number of divergent transitions, the effective sample size (ESS) for each estimated parameter (> 1000), and posterior predictive checks with the ShinyStan R package (Gabry et al., 2023). In addition, the model fits for each experiment were visually assessed (Figs. S1–S2). Finally, the median estimates for k_{600} and K_{600} were visualized in $\log(k_{600})$–$\log(Q)$ or $\log(K_{600})$–$\log(Q)$ space, respectively, along with 1000 Markov chain–Monte Carlo (MCMC) estimates of the $\log(k_{600})$–$\log(Q)$ or $\log(K_{600})$–$\log(Q)$ relationship, respectively. If an estimate of k_{600} and K_{600} fell outside the overall Q relationship and if that experiment's model fits showed signs of being unduly influenced by unrealistic gas-loss patterns (e.g., very little decline indicating the study reach was too short, an abrupt decline indicating improper mixing), the experiment was assessed for the QC flags described above. If a QC flag had previously been assigned, then that experiment was removed (e.g., it was identified as an outlier and could be attributed to experimental error), and the model was rerun without that experiment.

2.4 Recommended estimates

The processing pipeline outlined above in Sect. 2.3 resulted in both un-pooled frequentist and Bayesian estimates of k_{600} and K_{600}, both with and without salt corrections. We include outputs from all four approaches in the dataset for completeness and to allow future users to decide which estimates best fit their needs and to compare the two approaches. The complete dataset is available in the gasExchange_ds_v2.csv file (Aho et al., 2024).

During data processing, we found that the NaCl and NaBr concentration data also could introduce errors and uncertainties into our estimates of k_{600} and K_{600}. For instance, background concentrations at a single station were occasionally so high that contamination was the likely explanation. Further, sometimes samples taken during the constant-rate injection could vary across the reach in unpredictable ways (e.g., increases across the reach, random peaks along the reach instead of the expected stable, declining concentrations), which was likely the result of incomplete mixing with the water column. In many cases, the quality of the salt-corrected SF_6 data precluded Bayesian-model convergence. Through assessing the gas-loss plots and salt concentration declines for all experiments and the failures to produce model convergence for salt-corrected data, we determined that salt corrections had the strong potential to either introduce errors into or preclude estimates of k_{600} and K_{600}. Therefore, we suggest only using salt-corrected data when clearly necessary (e.g., obvious lateral inflow) and possible in terms of data quality and model convergence. We determined that salt correction was important for five sites: Como Creek (COMO), Rio Cupeyes (CUPE), Rio Yahuecas (GUIL), Martha Creek (MART), and Walker Branch (WALK). Notably, several of these sites have lateral inflows within the study reach under certain hydrologic conditions, which explains the necessity for the salt correction. For completeness, our dataset includes estimates for both uncorrected and salt-corrected k_{600} and K_{600} when a salt correction is possible.

In addition to the complete dataset of all estimates (i.e., estimates from both frequentist and Bayesian approaches for both uncorrected and salt-corrected data), we also include a curated dataset of recommended estimates of k_{600} and K_{600}. These recommended values are called "best_k600_mPerDay" and "best_K600_perDay" in the gasExchange_ds_v2.csv file. In all cases, the curated selection uses the Bayesian estimates because pooling across experiments and the use of informative priors resulted in more meaningful estimates than the non-Bayesian approach. The choice of whether we recommend an uncorrected or salt-corrected estimate stems from examining the relationships between uncorrected or salt-corrected estimates (Fig. S3).

3 Data description

3.1 Hydraulics

Our processing pipeline included calculating hydraulic parameters (v and $\overline{z}$) for each of the NaCl injections and measurements of Q and $\overline{w}$. These variables (v, $\overline{z}$, Q, and $\overline{w}$) for each NaCl release are available in the hydraulics_v2.csv file (Aho et al., 2024). Here, we present those data in terms of at-a-station hydraulic geometries, which are commonly used to quantify reach-specific relationships between Q and $\overline{w}$, $\overline{z}$, and v (Leopold and Maddock, 1953):

$$\overline{w} = aQ^b \tag{7}$$

$$\overline{z} = cQ^f \tag{8}$$

$$v = kQ^m. \tag{9}$$

In log–log space, these exponential relationships become linear relationships (e.g., $\overline{w} = aQ^b$ becomes $\log(\overline{w}) = \log(a) + b \times \log(Q)$), where the exponent is the slope log-linear relationship. Future users of NEON data can use these relationships along with discharge values from either the Continuous discharge data product (DP4.00130.001) or the Discharge field collection (DP1.20048.001) to approximate $\overline{w}$, $\overline{z}$, and v for NEON streams.

The hydraulic relationships are illustrated (Figs. 4–6, Table 2). These geometries leverage field measurements of $\overline{w}$ ($n = 783$) and Q ($n = 601$), estimates of v ($n = 618$) from NaCl injections, and estimates of $\overline{z}$ ($n = 581$) calculated from $Q/v\overline{w}$. The timing of these measurements is denoted on site-

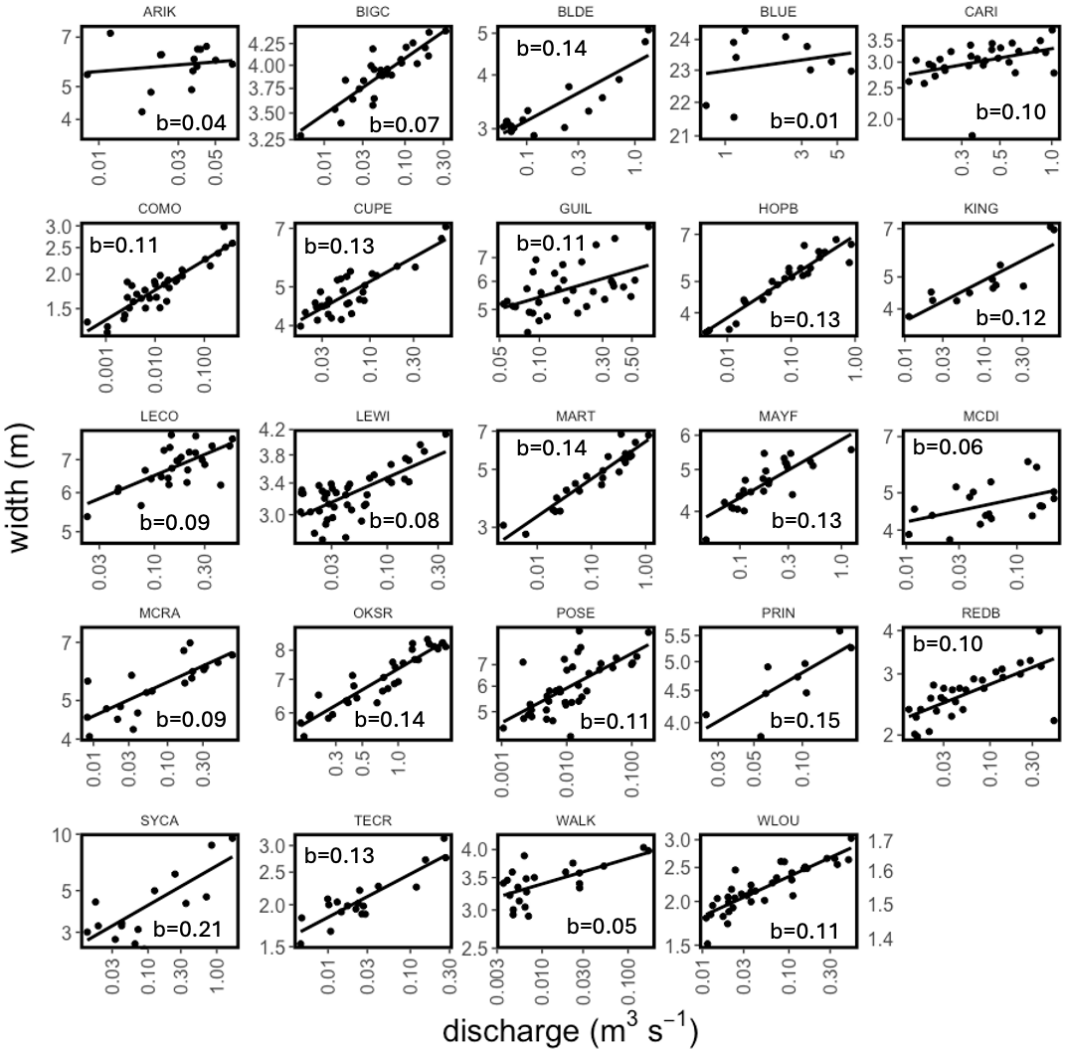

Figure 4. At-a-station hydraulic geometries for the relationship between Q and w. The exponent b of the power law relationship $\overline{w} = aQ^b$ is the linear slope of the relationship in log–log space and is denoted on each subplot.

specific hydrographs for each site (Fig. S4), and their coverage of site-specific Q ranges is illustrated on flow duration curves (Fig. S5). In general, $\overline{z}$–Q and v–Q relationships were the strongest, with all but three relationships having $R^2 > 0.5$ and relatively narrow 95 % confidence intervals around the coefficients from these relationships (Table 2). The $\overline{w}$–Q relationships are the weakest; 9 of the 24 sites have $R^2 < 0.5$ and large 95 % confidence intervals (Table 2). The $\overline{w}$–Q relationships may be weaker because our width estimates represent an average of 30 measurements across the ~ 500 m study reach. It is possible that this across-reach averaging contributes to the weaker relationships with Q and that perhaps the relationships would be stronger if the measurement was only taken at the same location as the Q measurement. However, this single-point approach would be less compatible with v measured of the entire reach and would alter the resulting calculations of $\overline{z}$.

We assess the quality of our hydraulic parameters by examining the product of the constants ($a \times c \times k$) and sum of the exponents ($b + f + m$) for unity on a site-by-site basis. These unity relationships stem from the fact that $Q = wzv$ (Leopold and Maddock, 1953). The products of the constants ranged from 0.93 to 1.04 and averaged 1.00; the site-specific sum of the exponents ranged from 0.96 to 1.01 and averaged 1.00. There was one instance where the product of the constants deviated more than 5 % from unity (0.93, PRIN). Pringle Creek (PRIN) is a semi-arid, intermittent stream in Texas, and so the deviation from unity may stem from logistical difficulties in measuring low and non-perennial stream flows (Seybold et al., 2023; Shanafield et al., 2021). However, the remainder of the sites had both products of constants and sums of exponents within 5 % of unity.

We assess the representativeness of our hydraulic parameters through comparison to literature values for the expo-

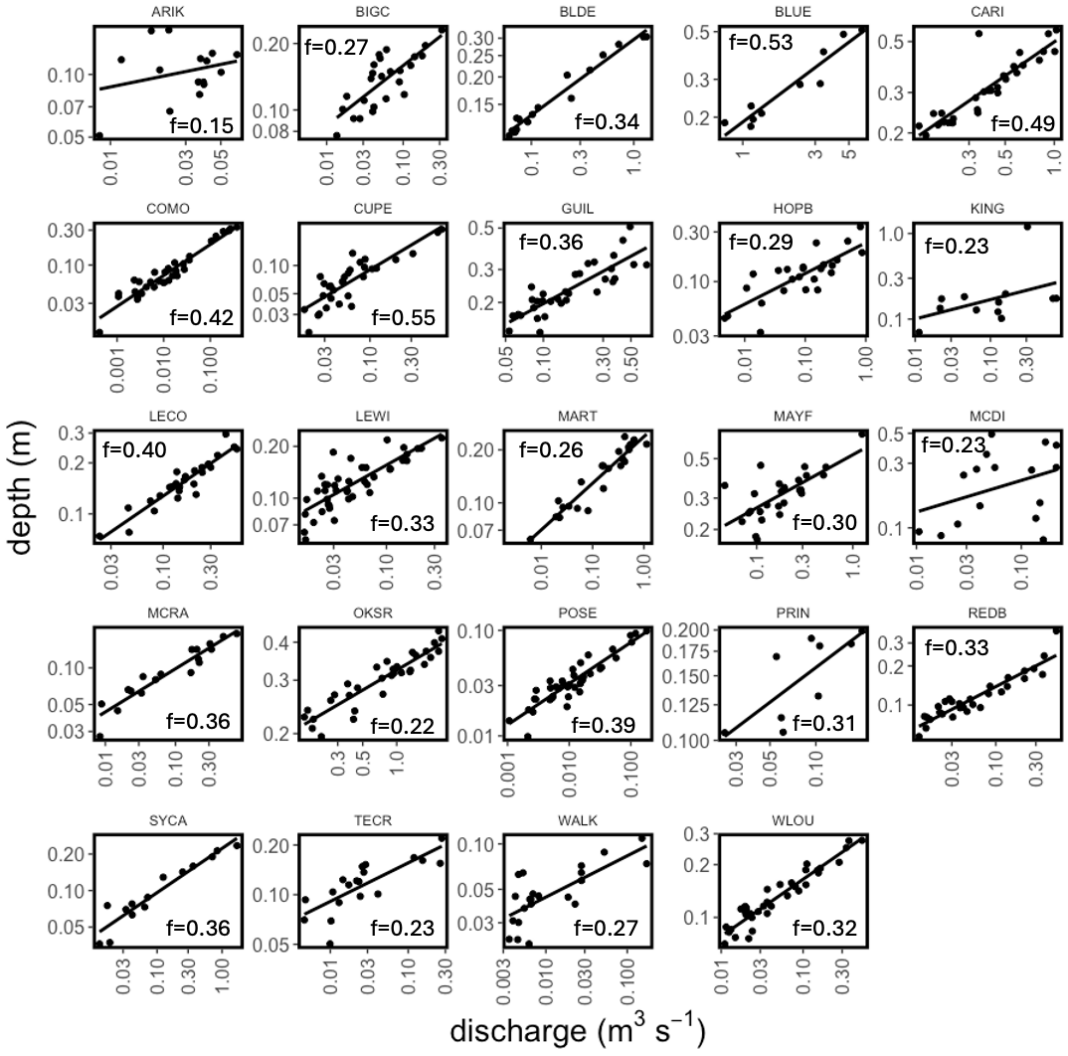

Figure 5. At-a-station hydraulic geometries for the relationship between Q and $\overline{z}$. The exponent f of the power law relationship $\overline{z} = cQ^f$ is the linear slope of the relationship in log–log space and is denoted on each subplot.

nents. Previous studies have shown large ranges for all three exponents, with ranges spanning 0–0.6 for b, 0–0.8 for f, and 0–0.8 for m (Park, 1977; Rhodes, 1977). In addition, exponents have not been shown to vary predictably with region or climate (Park, 1977) but rather with channel geometry (Ferguson, 1986). Our parameters fall within published ranges, and our average values for each exponent ($b = 0.11$, $f = 0.33$, $m = 0.56$) are similar to averages in other studies that span many streams ($b = 0.14$, $f = 0.30$; Morel et al., 2020; $b = 0.12$, $f = 0.37$, $m = 0.51$; Dingman and Afshari, 2018). In sum, the hydraulics dataset and associated hydraulic-geometry relationships presented here can be used to characterize $\overline{w}$, $\overline{z}$, and v for NEON streams.

3.2 k_{600} and K_{600} estimates

As described above, k_{600} was estimated in two ways: (1) via an unpooled frequentist approach using the `def.calc.reaeration()` function to estimate k_{600} independently for each experiment and (2) via a partially pooled Bayesian approach that partially pooled experiments from the same site according to Q. Both approaches were attempted for raw SF_6 concentrations and salt-corrected SF_6 concentrations. Salt-corrected SF_6 concentrations are only recommended for the five sites mentioned above (COMO, CUPE, GUIL, MART, WALK). All estimates are available in the gasExchange_ds_v2.csv file (Aho et al., 2024).

The relationship between the partially pooled and unpooled estimates (with salt correction when appropriate) is shown in Fig. 7. Any points falling above the 1 : 1 line are instances when partial pooling resulted in a lower estimate than no pooling, and vice versa. Overall, there are

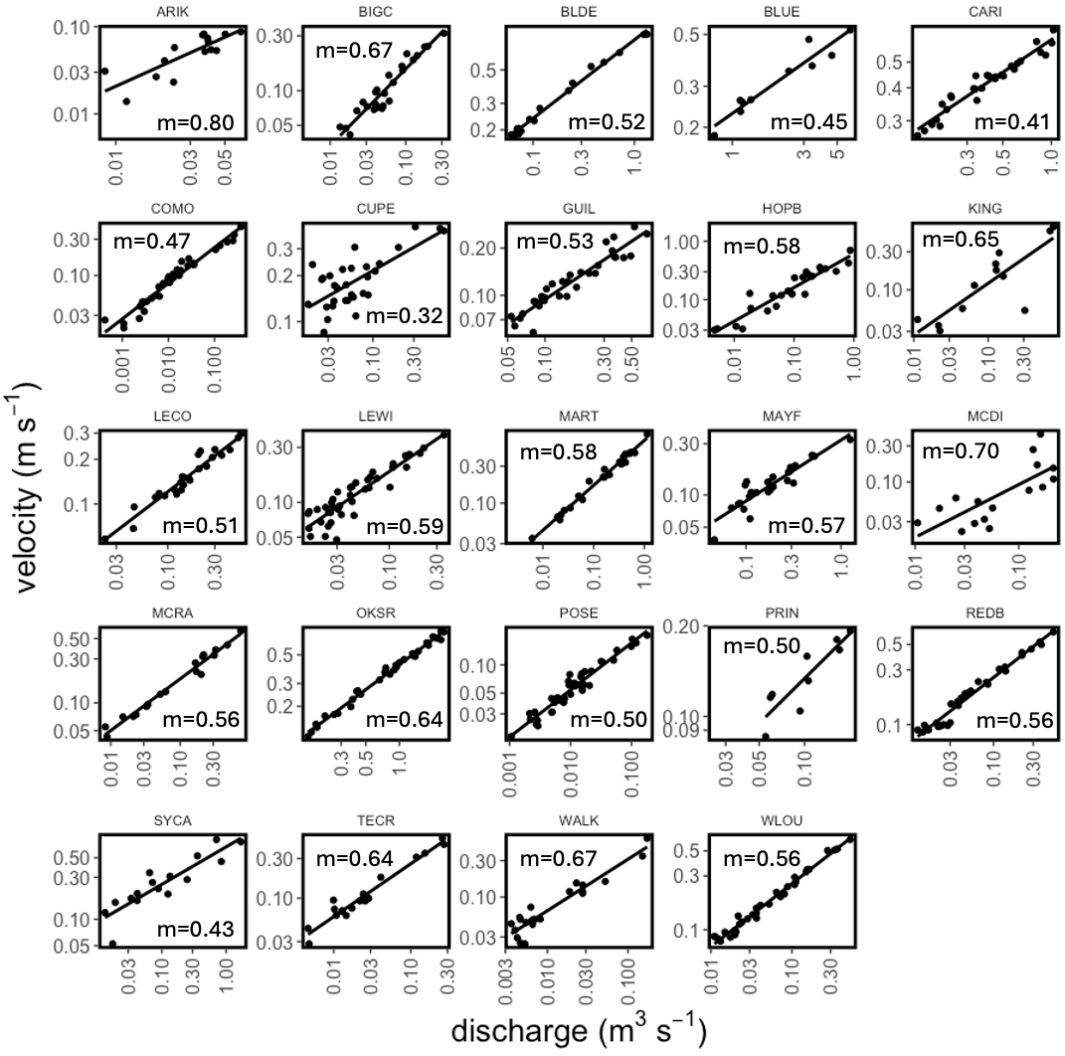

Figure 6. At-a-station hydraulic geometries for the relationship between Q and v. The exponent of the power law relationship $v = kQ^m$ is the linear slope of the relationship in log–log space and is denoted on each subplot.

instances where partially pooled estimates are both higher and lower than un-pooled estimates, suggesting that partial pooling successfully regularized estimates. This shrinkage is more obvious when both estimates are plotted against Q (Fig. 8). We made recommendations (best_k600_mPerDay and best_K600_perDay in the gasExchange_ds_v2.csv) of which estimates to use; this curated dataset includes only Bayesian estimates, and a salt correction was only recommended for the five sites where it was possible and necessary.

There are 339 estimates of k_{600} and K_{600} included in our recommended dataset (Fig. 9, Table 3) that span large Q ranges at each site (Figs. S4–S5). The number of estimates per site ranges from 4 (Kings Creek (KING) and Pringle Creek (PRIN)) to 29 (Posey Creek (POSE)). The issueLog.csv file documents the reason that 340 experiments did not successfully produce gas exchange estimates. These reasons are grouped into broad categories and summarized in Table S2. It is possible that some of the experiments that we removed could produce an estimate of k_{600} and K_{600} (e.g., if there was incomplete mixing at the first station, one could remove this station and only estimate k_{600} and K_{600} for Stations 2–4). However, this type of selective cleaning would have resulted in less comparable estimates (e.g., changing the length of the study reach), so we chose to include only the most comparable and high-quality experiments in this dataset.

The values for recommended estimates of k_{600} ranged from 0.1 to 142 m d^{-1}. LeConte Creek (LECO) had the highest mean k_{600} (mean ± SD: 53 ± 35 m d^{-1}), while Pringle Creek (PRIN) had the lowest mean k_{600} (mean ± SD: 1.1 ± 0.1 m d^{-1}). Lower Hop Brook (HOPB) had the widest spread of k_{600} values, with estimates ranging almost 2 orders of magnitude (1.5–124 m d^{-1}), while Pringle Creek (PRIN) had the smallest spread, with estimates only ranging from 0.9 to

Table 2. Coefficients and exponents from at-a-station hydraulic geometries. The 95 % confidence intervals for each coefficient and exponents are shown. In addition, the R^2 values from the log-linear relationships are also presented.

	$w = aQ^b$					$\bar{z} = cQ^f$					$v = kQ^m$				
Site	a	95 % CI	b	95 % CI	R^2	c	95 % CI	f	95 % CI	R^2	k	95 % CI	m	95 % CI	R^2
ARIK	6.7	(3.9,11)	0.04	(−0.11,0.19)	0.03	0.18	(0.06,0.56)	0.15	(−0.17,0.48)	0.08	0.84	(0.24,2.9)	0.80	(0.46,1.2)	0.66
BIGC	4.8	(4.6,5)	0.07	(0.05,0.08)	0.77	0.30	(0.22,0.4)	0.27	(0.18,0.37)	0.60	0.72	(0.55,0.95)	0.67	(0.58,0.76)	0.91
BLDE	4.3	(3.9,4.6)	0.14	(0.1,0.17)	0.78	0.30	(0.28,0.32)	0.34	(0.31,0.38)	0.97	0.79	(0.75,0.83)	0.52	(0.49,0.55)	0.99
BLUE	23	(22,24)	0.01	(−0.03,0.06)	0.06	0.19	(0.17,0.22)	0.53	(0.4,0.67)	0.91	0.23	(0.21,0.25)	0.45	(0.35,0.56)	0.92
CARI	3.3	(3,3.6)	0.10	(0.01,0.18)	0.16	0.50	(0.45,0.55)	0.49	(0.39,0.59)	0.80	0.61	(0.58,0.64)	0.41	(0.37,0.45)	0.94
COMO	2.9	(2.6,3.1)	0.11	(0.09,0.13)	0.82	0.51	(0.41,0.63)	0.42	(0.38,0.47)	0.92	0.68	(0.57,0.82)	0.47	(0.43,0.51)	0.95
CUPE	6.9	(6.3,7.5)	0.13	(0.1,0.16)	0.73	0.32	(0.22,0.47)	0.55	(0.42,0.68)	0.72	0.45	(0.32,0.63)	0.32	(0.2,0.44)	0.52
GUIL	7	(6.1,7.9)	0.11	(0.04,0.18)	0.26	0.45	(0.39,0.53)	0.36	(0.28,0.45)	0.73	0.32	(0.28,0.36)	0.53	(0.46,0.6)	0.90
HOPB	6.9	(6.6,7.3)	0.13	(0.11,0.15)	0.89	0.24	(0.18,0.31)	0.29	(0.2,0.39)	0.64	0.61	(0.47,0.79)	0.58	(0.49,0.66)	0.89
KING	6.5	(5.7,7.4)	0.12	(0.08,0.17)	0.76	0.28	(0.12,0.67)	0.23	(−0.1,0.55)	0.20	0.54	(0.24,1.2)	0.65	(0.35,0.95)	0.70
LECO	8	(7.4,8.6)	0.09	(0.05,0.13)	0.47	0.32	(0.28,0.37)	0.40	(0.34,0.47)	0.87	0.39	(0.35,0.43)	0.51	(0.45,0.56)	0.93
LEWI	4.2	(3.9,4.5)	0.08	(0.06,0.11)	0.51	0.33	(0.26,0.42)	0.33	(0.25,0.4)	0.66	0.72	(0.56,0.93)	0.59	(0.51,0.67)	0.84
MART	6.4	(6,6.8)	0.14	(0.12,0.16)	0.89	0.24	(0.22,0.26)	0.26	(0.22,0.3)	0.90	0.65	(0.6,0.7)	0.58	(0.55,0.61)	0.99
MAYF	5.9	(5.4,6.3)	0.13	(0.1,0.17)	0.68	0.53	(0.42,0.66)	0.30	(0.17,0.42)	0.50	0.32	(0.27,0.4)	0.57	(0.46,0.68)	0.83
MCDI	5.6	(4.7,6.6)	0.06	(0,0.12)	0.22	0.38	(0.14,1)	0.23	(−0.11,0.57)	0.13	0.46	(0.17,1.3)	0.70	(0.35,1)	0.57
MCRA	6.8	(6.1,7.5)	0.09	(0.05,0.12)	0.61	0.22	(0.19,0.27)	0.36	(0.29,0.42)	0.90	0.66	(0.58,0.75)	0.56	(0.52,0.61)	0.98
OKSR	7.3	(7.2,7.5)	0.14	(0.12,0.16)	0.87	0.32	(0.31,0.33)	0.22	(0.18,0.25)	0.85	0.42	(0.41,0.43)	0.64	(0.62,0.67)	0.99
POSE	9.7	(8.1,12)	0.11	(0.07,0.15)	0.46	0.19	(0.15,0.25)	0.39	(0.33,0.45)	0.84	0.54	(0.45,0.66)	0.50	(0.46,0.54)	0.94
PRIN	6.7	(5.1,8.9)	0.15	(0.04,0.25)	0.61	0.33	(0.17,0.61)	0.31	(0.07,0.56)	0.57	0.42	(0.24,0.72)	0.50	(0.26,0.73)	0.79
REDB	3.5	(3.1,4)	0.10	(0.06,0.14)	0.49	0.30	(0.26,0.35)	0.33	(0.28,0.39)	0.86	0.94	(0.84,1.1)	0.56	(0.53,0.6)	0.97
SYCA	6.8	(5.2,8.9)	0.21	(0.11,0.31)	0.65	0.22	(0.18,0.27)	0.36	(0.29,0.44)	0.91	0.67	(0.48,0.93)	0.43	(0.3,0.55)	0.80
TECR	3.3	(2.9,3.8)	0.13	(0.09,0.16)	0.79	0.27	(0.19,0.38)	0.23	(0.14,0.33)	0.62	1.10	(0.85,1.5)	0.64	(0.57,0.71)	0.95
WALK	4.3	(3.8,4.9)	0.05	(0.02,0.08)	0.43	0.16	(0.09,0.27)	0.27	(0.16,0.39)	0.55	1.50	(0.92,2.4)	0.67	(0.57,0.78)	0.90
WLOU	3.1	(2.8,3.3)	0.11	(0.09,0.14)	0.74	0.35	(0.31,0.39)	0.32	(0.29,0.36)	0.91	0.93	(0.85,1)	0.56	(0.53,0.58)	0.98

Table 3. Mean, standard deviation (SD), minimum, maximum, and count for k_{600} ($\mathrm{m\,d^{-1}}$) and K_{600} ($\mathrm{d^{-1}}$) estimates by site.

		k_{600} ($\mathrm{m\,d^{-1}}$)				K_{600} ($\mathrm{d^{-1}}$)			
Site	n	mean	SD	min	max	mean	SD	min	max
BIGC	22	2.1	0.9	0.7	4.1	15.6	7.8	6.2	39.9
BLDE	11	5.9	6.2	1.7	23.4	33	19.9	12.1	83.1
CARI	16	9.5	8.3	3.4	35.6	31.7	32.5	6.1	140.9
COMO	17	26.8	32.1	2.7	94.8	182.7	91.9	66.6	377.3
CUPE	26	6.5	3.1	3.1	15.8	104.7	33.5	47.3	190.1
GUIL	15	9.3	6	3.6	22.4	39.7	21.7	15	83.1
HOPB	19	15	27.8	1.6	123.6	90.7	80.4	29.5	367.6
KING	4	4.3	2	2.8	7.2	34.5	25.6	12.2	62.4
LECO	10	53.2	35.4	21.4	142.2	275.7	94.4	156	481.4
LEWI	21	2.2	1	0.9	4.6	19.2	7.1	9.1	34.5
MART	7	1.2	1.2	0.1	3.4	12.3	13.3	1.3	35.7
MAYF	7	12.3	11	2.8	34.3	39	40.5	9.3	126.9
MCDI	6	4.8	0.8	3.5	5.7	26.8	16.7	10.2	53.2
MCRA	16	10.6	9.9	1.2	33.9	87.8	46.5	27.6	185.9
OKSR	21	4.8	5.8	1.4	29.4	15.4	14.4	4.2	74
POSE	29	3.8	2.6	0.7	11	108.6	35.5	48.9	187.4
PRIN	4	1.1	0.1	0.9	1.2	7.2	1.7	5.7	9.2
REDB	25	14.1	11.3	3	53.9	102.9	40.2	42.4	181.4
SYCA	11	2.3	2.3	0.3	8	30	23.8	3.7	64.6
TECR	15	12	8.4	3.2	28.7	93.5	42	33.9	181.9
WALK	9	2.1	1.1	0.1	3.6	59.9	22.2	6.6	82.2
WLOU	28	31.6	26	9.6	112.9	199.6	83.4	93.8	410

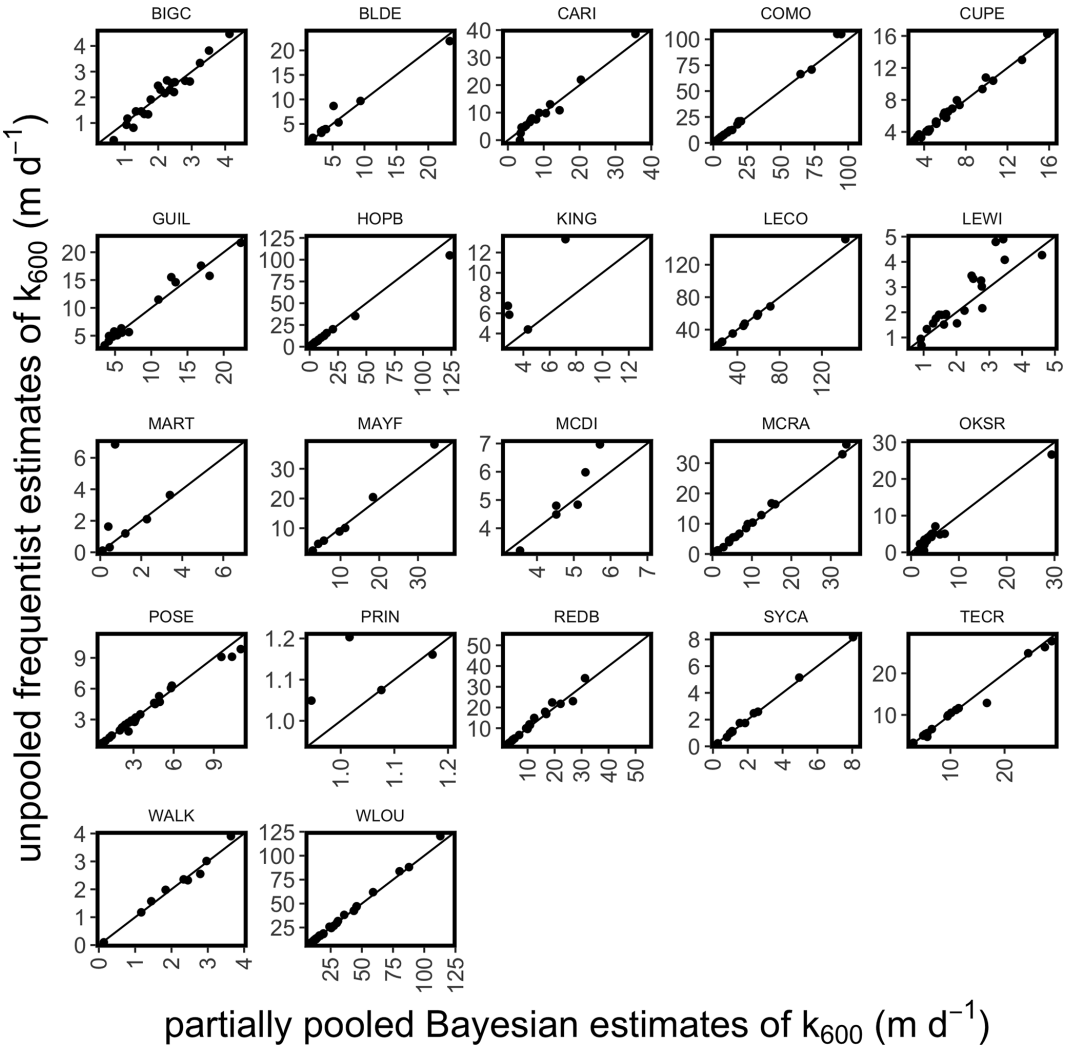

Figure 7. Comparison of partially pooled Bayesian and unpooled frequentist estimates of k_{600}. Black 1 : 1 lines overlay the points for reference.

1.2 m d^{-1}. The values for recommended estimates of K_{600} range from 1.3 to 481 d^{-1}. Like for k_{600}, LeConte Creek (LECO) had the highest mean K_{600} (mean ± SD: 276 ± 94 d^{-1}), while Pringle Creek (PRIN) had the lowest mean K_{600} (mean ± SD: 7.0 ± 1.9 d^{-1}). Also, Lower Hop Brook (HOPB) had the widest spread of K_{600} values, with estimates ranging from 30 to 368 d^{-1}, while Pringle Creek (PRIN) had the smallest spread, with estimates ranging from 5.3 to 9.3 d^{-1}. These ranges, in part, reflect the various ranges of Q captured at each site (Table S3). HOPB was among the sites with the largest range of Q captured, while PRIN was among the sites with the smallest Q range captured (Table S3). Overall, this large compilation of k_{600} and K_{600} estimates indicates high variability both across and within sites.

Finally, to allow future users to scale k_{600} and K_{600} with Q, we include both the slope and intercept for the k_{600}–Q and K_{600}–Q relationships (Table 4) and the stanfit objects for the Bayesian models ("Other Entities" in the data release). The slope and intercept will allow future users a straightforward way to scale k_{600} or K_{600} as a function of Q at each site. The stanfit objects, on the other hand, will allow future users to sample from the posterior distribution of slope and intercept to assess uncertainty in the scaling relationships.

4 Code and data availability

The reaRate R package is available at https://doi.org/10.5281/zenodo.12786089 (Cawley et al., 2024). The dataset of hydraulic parameters and gas exchange estimates is available from the Environmental Data Initiative: https://doi.org/10.6073/pasta/18dcc1871ee71cf0b69f2ee4082839d0 (Aho et al., 2024).

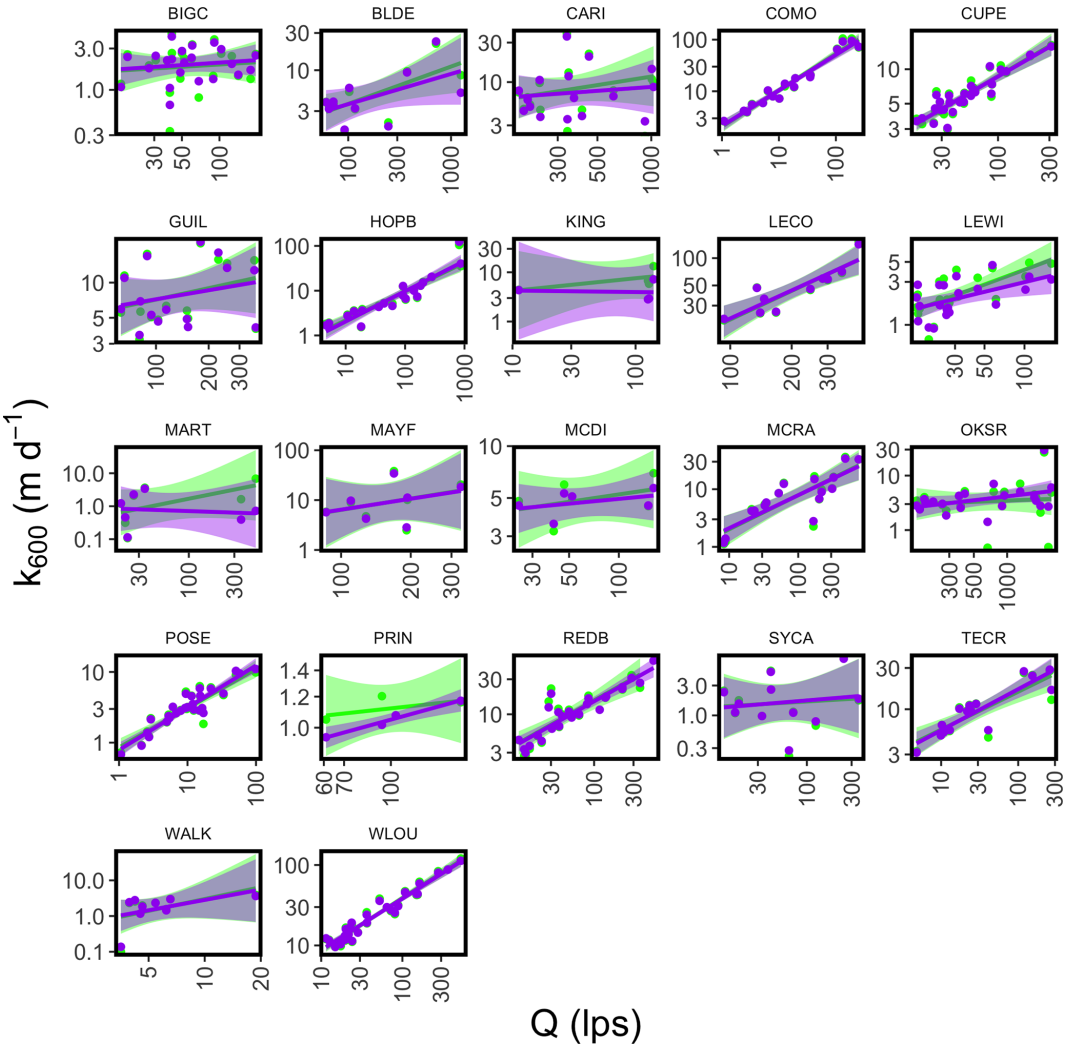

Figure 8. Relationship between Q and partially pooled Bayesian and unpooled frequentist estimates of k_{600}. The unpooled estimates are shown in green, with a green regression line with 95 % confidence intervals, while the partially pooled estimates are shown in purple, with a purple regression line with 95 % confidence intervals.

5 Conclusions

Here, we present 339 estimates of gas exchange velocity (k_{600}) and gas exchange rate (K_{600}) from 22 NEON streams. To our knowledge, this dataset is the largest compilation of gas exchange estimates from standardized tracer-gas experiments (i.e., standardized methods across all experiments and sites) published to date. Given the wide geographic spread of NEON streams (e.g., spanning Puerto Rico to Alaska), this dataset will enable understanding of gas exchange across biomes. In addition, in our estimation process, we leverage new Bayesian multilevel models that allow estimates of gas exchange to be partially pooled by site according to Q; this modeling approach can be applied to future studies where repeat tracer-gas experiments are conducted to characterize gas exchange as a function of Q. Here, we also present relationships between discharge and gas exchange (i.e., k_{600}–Q and K_{600}–Q) from these models that will allow future users to scale k_{600} or K_{600} as a function of Q in NEON streams.

Regarding hydraulics, we present hydraulic geometries for 24 NEON streams. These geometries leverage field measurements of $\overline{w}$ and Q and estimate v and $\overline{z}$. The coefficients and exponents from at-a-station hydraulic geometries are presented and can be used in the future, along with Continuous discharge (DP4.00130.001), to estimate $\overline{w}$, v, and $\overline{z}$ at NEON streams. In sum, this large dataset could allow for quantification of both within- and across-reach variability in hydraulics and gas exchange in streams, which could be useful to modeling stream metabolism, greenhouse gas emissions, and other biogeochemical fluxes in NEON streams. In addition, this dataset may facilitate the development of new predictive models of gas exchange in small streams.

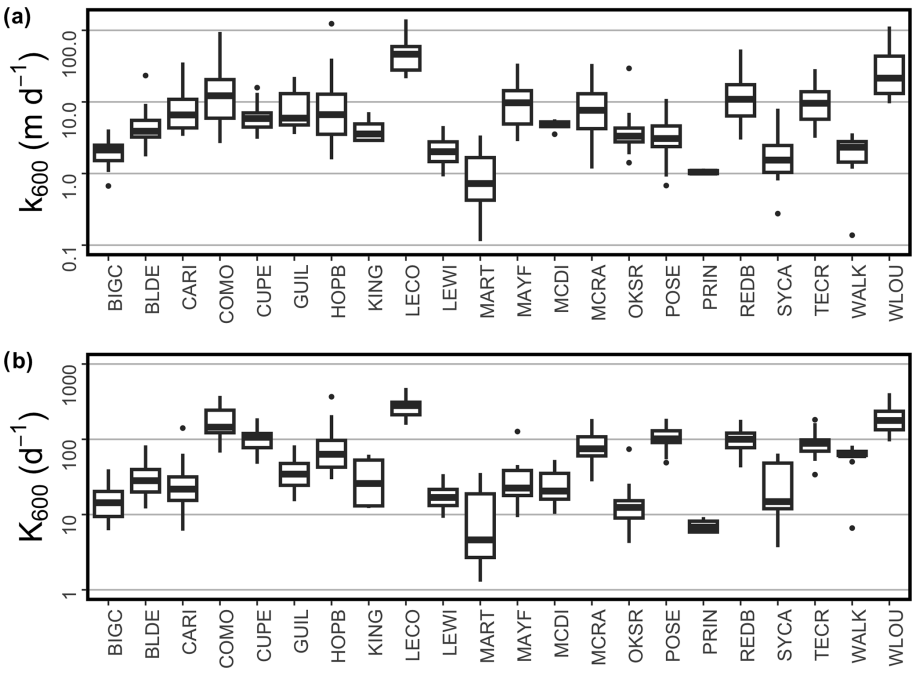

Figure 9. Box plots of the test estimates of **(a)** k_{600} and **(b)** K_{600} by site. Boxes represent the median and interquartile range (IQR), whiskers mark the lesser of first (third) quartile − (+) 1.5 × IQR or minimum/maximum, and points denote outliers more extreme than first (third) quartile − (+) 1.5 × IQR.

Table 4. Coefficients and exponents for k_{600}–Q and K_{600}–Q relationships. Estimates and standard deviations (SD) are given.

	$k_{600} = aQ^b$				$K_{600} = aQ^b$			
	a		b		a		b	
Site	Estimate	SD	Estimate	SD	Estimate	SD	Estimate	SD
BIGC	−0.31	1.55	0.11	0.18	3.55	1.57	−0.11	0.19
BLDE	−2.11	2.27	0.38	0.24	2.88	2.15	0.05	0.23
CARI	0.06	3.51	0.19	0.34	6.50	3.69	−0.32	0.36
COMO	−2.30	0.34	0.69	0.05	3.17	0.32	0.27	0.04
CUPE	−2.74	0.54	0.54	0.07	4.84	0.92	−0.03	0.11
GUIL	−0.51	2.84	0.27	0.30	4.50	2.58	−0.10	0.28
HOPB	−3.83	0.64	0.67	0.07	0.94	0.48	0.39	0.05
KING	−1.97	2.47	0.38	0.25	0.06	2.76	0.36	0.30
LECO	−5.68	2.21	0.97	0.23	0.66	1.85	0.50	0.19
LEWI	−2.18	1.78	0.36	0.23	3.48	1.78	−0.07	0.23
MART	−0.55	4.34	0.03	0.55	3.82	4.34	−0.23	0.54
MAYF	−3.44	5.44	0.59	0.57	−0.04	5.46	0.35	0.57
MCDI	0.40	2.02	0.13	0.24	0.29	4.06	0.33	0.48
MCRA	−3.07	1.06	0.57	0.12	2.37	0.93	0.22	0.11
OKSR	−1.41	1.94	0.25	0.18	2.30	2.04	0.02	0.19
POSE	−2.90	0.36	0.60	0.05	3.21	0.37	0.21	0.05
PRIN	−2.69	0.88	0.30	0.10	2.37	0.97	−0.05	0.11
REDB	−2.99	0.70	0.63	0.08	1.97	0.60	0.30	0.07
SYCA	−0.73	2.67	0.14	0.32	5.15	2.77	−0.25	0.33
TECR	−1.47	0.63	0.48	0.08	2.61	0.71	0.23	0.09
WALK	−4.03	3.48	0.73	0.56	0.96	3.09	0.48	0.50
WLOU	−2.15	0.30	0.64	0.04	2.48	0.31	0.33	0.04

Supplement. The supplement related to this article is available online at: https://doi.org/10.5194/essd-16-5563-2024-supplement.

Author contributions. Conceptualization: KSA, KMC, RTH, ROH Jr., WKD, KJG. Methodology: KSA, KMC, RTH, ROH Jr. with support from all authors. Software: KSA, KMC, ROH Jr. Writing (original draft): KSA with support from all authors. Writing (review and editing): KSA, KMC, RTH, ROH Jr., WKD, KJG.

Competing interests. The contact author has declared that none of the authors has any competing interests.

Disclaimer. Publisher's note: Copernicus Publications remains neutral with regard to jurisdictional claims made in the text, published maps, institutional affiliations, or any other geographical representation in this paper. While Copernicus Publications makes every effort to include appropriate place names, the final responsibility lies with the authors.

Acknowledgements. The National Ecological Observatory Network (NEON) is a programme sponsored by the National Science Foundation and operated under cooperative agreement by Battelle. This material is based in part upon work supported by the National Science Foundation through the NEON programme. The idea for this dataset initially came from meetings of the NEON Reaeration Technical Working Group.

Review statement. This paper was edited by Yuanzhi Yao and reviewed by Chunlin Song and Liwei Zhang.

References

Aho, K. S., Cawley, K., Hensley, R., Hall, R. O., Dodds, W., and Goodman, K.: Gas exchange velocities (k600), gas exchange rates (K600), and hydraulic geometries for streams and rivers derived from the NEON Reaeration field and lab collection data product (DP1.20190.001) ver 2, Environmental Data Initiative [data set], https://doi.org/10.6073/pasta/18dcc1871ee71cf0b69f2ee4082839d0, 2024.

Appling, A. P., Hall, R. O., Yackulic, C. B., and Arroita, M.: Overcoming Equifinality: Leveraging Long Time Series for Stream Metabolism Estimation, J. Geophys. Res.-Biogeo., 123, 624–645, https://doi.org/10.1002/2017JG004140, 2018.

Aristegi, L., Izagirre, O., and Elosegi, A.: Comparison of several methods to calculate reaeration in streams, and their effects on estimation of metabolism, Hydrobiologia, 635, 113–124, https://doi.org/10.1007/s10750-009-9904-8, 2009.

Cawley, K., Aho, K. S., and Hall, R. O.: reaRate R package, NEONScience/NEON-reaeration: v0.0.2, Zenodo [code], https://doi.org/10.5281/zenodo.12786089, 2024.

Churchill, M. A., Elmore, H. L., and Buckingham, R. A.: The Prediction of Stream Reaeration Rates, in: Advances in Water Pollution Research, Elsevier, 89–136, https://doi.org/10.1016/B978-1-4832-8391-3.50015-4, 1964.

Cole, J. J. and Caraco, N. F.: Atmospheric exchange of carbon dioxide in a low-wind oligotrophic lake measured by the addition of SF6, Limnol. Oceanogr., 43, 647–656, https://doi.org/10.4319/lo.1998.43.4.0647, 1998.

Dingman, S. L. and Afshari, S.: Field verification of analytical at-a-station hydraulic-geometry relations, J. Hydrol. (Amst), 564, 859–872, https://doi.org/10.1016/j.jhydrol.2018.07.020, 2018.

Ferguson, R. I.: Hydraulics and hydraulic geometry, Prog. Phys. Geogr.-Earth and Environment, 10, 1–31, https://doi.org/10.1177/030913338601000101, 1986.

Gabry, J., Veen, D., Team, S. D., Andreae, M., Betancourt, M., Carpenter, B., Gao, Y., Gelman, A., Goodrich, B., Lee, D., Song, D., and Trangucci, R.: shinystan: Interactive visual and numerical diagnostics and posterior analysis for Bayesian models, R package version 2.6.0, CRAN [code], https://CRAN.R-project.org/package=shinystan (last access: 8 May 2024), 2023.

Genzoli, L. and Hall, R. O.: Shifts in Klamath River metabolism following a reservoir cyanobacterial bloom, Freshwater Sci., 35, 795–809, https://doi.org/10.1086/687752, 2016.

Hall, R. O. and Hotchkiss, E. R.: Stream Metabolism, in: Methods in Stream Ecology, Academic Press, 219–233, 2017.

Hall, R. O. and Ulseth, A. J.: Gas exchange in streams and rivers, WIREs Water, 7, 1–18, https://doi.org/10.1002/wat2.1391, 2020.

Hall, R. O., Tank, J. L., Baker, M. A., Rosi-Marshall, E. J., and Hotchkiss, E. R.: Metabolism, Gas Exchange, and Carbon Spiraling in Rivers, Ecosystems, 19, 73–86, https://doi.org/10.1007/s10021-015-9918-1, 2016.

Ho, D. T., Schlosser, P., and Orton, P. M.: On Factors Controlling Air-Water Gas Exchange in a Large Tidal River, Estuar. Coast., 34, 1103–1116, https://doi.org/10.1007/s12237-011-9396-4, 2011.

Hornberger, G. M. and Kelly, M. G.: Atmospheric Reaeration in a River Using Productivity Analysis, J. Environ. Eng. Div., 101, 729–739, https://doi.org/10.1061/JEEGAV.0000398, 1975.

Jähne, B., Münnich, K. O., Bösinger, R., Dutzi, A., Huber, W., and Libner, P.: On the parameters influencing air-water gas exchange, J. Geophys. Res.-Oceans, 92, 1937–1949, https://doi.org/10.1029/JC092iC02p01937, 1987.

Leopold, L. B. and Maddock Jr., T.: The Hydraulic Geometry of Stream Channels and Some Physiographic Implications, Geological Survey Professional Paper 252, United States Government Printing Office, Washington, 1953.

Liu, S., Kuhn, C., Amatulli, G., Aho, K., Butman, D. E., Allen, G. H., Lin, P., Pan, M., Yamazaki, D., Brinkerhoff, C., Gleason, C., Xia, X., and Raymond, P. A.: The importance of hydrology in routing terrestrial carbon to the atmosphere via global streams and rivers, P. Natl. Acad. Sci. USA, 119, 1–9, https://doi.org/10.1073/pnas.2106322119, 2022.

Maurice, L., Rawlins, B. G., Farr, G., Bell, R., and Gooddy, D. C.: The Influence of Flow and Bed Slope on Gas Transfer in Steep Streams and Their Implications for Evasion of CO_2, J. Geophys. Res.-Biogeo., 122, 2862–2875, https://doi.org/10.1002/2017JG004045, 2017.

McDowell, M. J. and Johnson, M. S.: Gas Transfer Velocities Evaluated Using Carbon Dioxide as a Tracer Show High Streamflow to Be a Major Driver of Total CO_2 Evasion Flux for a

Headwater Stream, J. Geophys. Res.-Biogeo., 123, 2183–2197, https://doi.org/10.1029/2018JG004388, 2018.

Morel, M., Booker, D. J., Gob, F., and Lamouroux, N.: Consistent Theoretical and Empirical Predictions of at-a-Station Hydraulic Geometry Exponents in Stream Reaches, Water Resour. Res., 56, 1–16, https://doi.org/10.1029/2020WR027242, 2020.

NEON: Discharge field collection (DP1.20048.001) RELEASE-2023, NEON [data set], https://doi.org/10.48443/tys0-ze83, 2023a.

NEON: Reaeration field and lab collection (DP.20190.001) RELEASE-2023, NEON [data set], https://doi.org/10.48443/bk29-6c91, 2023b.

NEON: Discharge field collection (DP1.20048.001) RELEASE-2024, NEON [data set], https://doi.org/10.48443/3746-1981, 2024a.

NEON: Reaeration field and lab collection (DP1.20190.001) RELEASE-2024, NEON [data set], https://doi.org/10.48443/4z25-4b94, 2024b.

O'Connor, D. J. and Dobbins, W. E.: Mechanism of Reaeration in Natural Streams, T. Am. Soc. Civil Eng., 123, 641–666, https://doi.org/10.1061/TACEAT.0007609, 1958.

Park, C. C.: World-wide variations in hydraulic geometry exponents of stream channels: An analysis and some observations, J. Hydrol. (Amst), 33, 133–146, https://doi.org/10.1016/0022-1694(77)90103-2, 1977.

Rathbun, R. E.: Reaeration Coefficients of Streams – State-of-the-Art, J. Hydraul. Div., 103, 409–424, https://doi.org/10.1061/JYCEAJ.0004734, 1977.

Raymond, P. A., Zappa, C. J., Butman, D., Bott, T. L., Potter, J., Mulholland, P., Laursen, A. E., McDowell, W. H., and Newbold, D.: Scaling the gas transfer velocity and hydraulic geometry in streams and small rivers, Limnol. Oceanogr.-Fluids and Environments, 2, 41–53, https://doi.org/10.1215/21573689-1597669, 2012.

R Core Team: R: A language and environment for statistical computing, R Foundation for Statistical Computing, Vienna, Austria, https://www.R-project.org/, 2023.

Rhodes, D. D.: The b-f-m diagram; graphical representation and interpretation of at-a-station hydraulic geometry, Am. J. Sci., 277, 73–96, https://doi.org/10.2475/ajs.277.1.73, 1977.

Riley, A. J. and Dodds, W. K.: Whole-stream metabolism: Strategies for measuring and modeling diel trends of dissolved oxygen, Freshwater Sci., 32, 56–69, https://doi.org/10.1899/12-058.1, 2013.

Rocher-Ros, G., Stanley, E. H., Loken, L. C., Casson, N. J., Raymond, P. A., Liu, S., Amatulli, G., and Sponseller, R. A.: Global methane emissions from rivers and streams, Nature, 621, 530–535, https://doi.org/10.1038/s41586-023-06344-6, 2023.

Seybold, E. C., Bergstrom, A., Jones, C. N., Burgin, A. J., Zipper, S., Godsey, S. E., Dodds, W. K., Zimmer, M. A., Shanafield, M., Datry, T., Mazor, R. D., Messager, M. L., Olden, J. D., Ward, A., Yu, S., Kaiser, K. E., Shogren, A., and Walker, R. H.: How low can you go? Widespread challenges in measuring low stream discharge and a path forward, Limnol. Oceanogr. Lett., 8, 804–811, https://doi.org/10.1002/lol2.10356, 2023.

Shanafield, M., Bourke, S. A., Zimmer, M. A., and Costigan, K. H.: An overview of the hydrology of non-perennial rivers and streams, Wiley Interdisciplinary Reviews: Water, 8, 1–25, https://doi.org/10.1002/wat2.1504, 2021.

Stan Development Team: RStan: the R interface to Stan, R package version 2.26.22, https://mc-stan.org/ (last access: 8 May 2024), 2023.

Ulseth, A. J., Hall, R. O., Boix Canadell, M., Madinger, H. L., Niayifar, A., and Battin, T. J.: Distinct air–water gas exchange regimes in low- and high-energy streams, Nat. Geosci., 12, 259–263, https://doi.org/10.1038/s41561-019-0324-8, 2019.

Wanninkhof, R.: Relationship between wind speed and gas exchange over the ocean, J. Geophys. Res., 97, 7373–7382, https://doi.org/10.1029/92JC00188, 1992.

Wanninkhof, R., Ledwell, J. R., and Broecker, W. S.: Gas exchange-wind speed relation measured with sulfur hexafluoride on a lake, Science, 227, 1224–1226, https://doi.org/10.1126/science.227.4691.1224, 1985.

Zappa, C. J., McGillis, W. R., Raymond, P. A., Edson, J. B., Hintsa, E. J., Zemmelink, H. J., Dacey, J. W. H., and Ho, D. T.: Environmental turbulent mixing controls on air-water gas exchange in marine and aquatic systems, Geophys. Res. Lett., 34, L10601, https://doi.org/10.1029/2006GL028790, 2007.